WIND TUNNEL TEST OF SINGLE-ROTOR LIFT-OFFSET DUE TO DIFFERENTIAL FLAPS

Hideaki Sugawara, sugawara.hideaki@jaxa.jp, Japan Aerospace Exploration Agency (Japan)
Noboru Kobiki, kobiki@chofu.jaxa.jp, Japan Aerospace Exploration Agency (Japan)
Yasutada Tanabe, tan@chofu.jaxa.jp, Japan Aerospace Exploration Agency (Japan)
Masafumi Sasaki, sasaki.masafumi@subaru.co.jp, SUBARU CORPORATION (Japan)
Ayumi Higo, higo.ayumi@subaru.co.jp, SUBARU CORPORATION (Japan)
Mizuki Nakamura, nakamura.mizuki@subaru.co.jp, SUBARU CORPORATION (Japan)

Abstract

A single-rotor lift-offset system for a winged compound helicopter is evaluated at JAXA 2m x 2m low-speed wind tunnel in the closed test section using a flyable radio-controlled model rotorcraft. The single-rotor lift-offset is achieved utilizing flaps originally designed for download reduction during hovering flight on a winged compound helicopter. Differential flaps on the left and right wings create a rolling moment on the wing-body to produce a lift-offset state of the rotor while the overall rotorcraft rolling moment is balanced. Two types of rotor blades, which are the optimized rotor blade for high advance-ratio flight and the reference UH-60A rotor blade, were tested to compare the effect of lift-offset on the overall aerodynamic performance. The tests were conducted at advance ratios of 0.3, 0.5, and 0.7. The test results show that the single-rotor lift-offset improves the overall effective lift-to-drag ratio as expected. Furthermore, the adverse yaw effect due to the differential flaps is observed from the test results of isolated wing-body.

1. INTRODUCTION

Compound helicopter is one of the high-speed rotorcraft concepts and is being studied for use in missions that require high-speed performance, such as emergency medical service (EMS) helicopters [1, 2]. However, rotorcrafts have many aerodynamic interference issues [3], affecting the aerodynamic performance of their components and flight handling quality. When the rotorcraft cannot achieve the expected performance due to aerodynamic interference, it is noted that a redesign of the rotorcraft can be required, thereby increasing the cost of development [4].

The main rotor causes aerodynamic interference with many components and has undesirable aerodynamic effects in most cases. Compound helicopters generally have more components compared to conventional helicopters, such as propellers and fixed wings, that create new aerodynamic interferences between the main rotor and the additional components. Therefore, it is essential to understand the impact of aerodynamic interferences on the aerodynamic performance of the compound helicopter and investigate technologies to achieve higher aerodynamic performance. This paper focuses on the aerodynamic interference issues between the rotor and fixed wing and examines the technology to improve the aerodynamic performance of winged compound helicopters.

The compound helicopters operate at higher speeds than conventional helicopters, resulting in a higher advance ratio of the rotor. Therefore, the aerodynamic environment around the rotor is considerably different, such as the extended reverse flow region on the blade retreating side and the rotor wake including the tip vorticity location. The experimental and numerical studies to investigate the effect of aerodynamic interference between the rotor and fixed wing under high advance ratios have been reported by several researchers [5-9].

Brouwers et al. investigated the rotor/wing aerodynamic interference on a winged compound helicopter through a wind tunnel test up to the advance ratio of 0.45 [5]. Frey et al. performed the numerical simulation using Computational Fluid Dynamics (CFD) to evaluate the mutual interference of the main rotor, fixed wings, and lateral rotors over the advance ratio of 0.5 based on RACER configuration [6]. The present authors also studied

the rotor/wing aerodynamic interactions experimentally and numerically in high advance ratios [7-9]. These studies provided interesting insights into aerodynamic interference between the rotor and the wing under high advance ratio conditions. Even though the rotor wake is parallel to the rotor tip-path plane, the rotor affects the aerodynamic performance of the wing significantly. This effect is more noticeable on the advancing side and is an asymmetric phenomenon. The rotor/wing aerodynamic interaction also remarkably reduces the overall performance of the rotorcraft. High aerodynamic performance can be achieved through optimal design, but performance degradation remains due to the aerodynamic interaction. Therefore, technologies are desired to achieve higher aerodynamic performance taking into the effect of interaction.

Lift-offset technology is a promising technology to enhance rotor performance and has been demonstrated in the coaxial rotor system [10-13]. For the single rotor system, a rolling moment of the rotor is required to create the lift-offset state. Thus, a system to cancel the rolling moment of the rotor is required to keep the rotorcraft roll attitude.

Reddinger and Gandhi studied the optimal trim states of a compound helicopter with an articulated rotor [14]. Differential ailerons enabled the lift-offset of a single rotor, and the overall effective lift-to-drag ratio of the rotorcraft was increased. At the University of Maryland, a single rotor with a half-wing was investigated experimentally and numerically [15-17]. The fixed-wing was mounted on the fuselage under the blade retreating side to create the rolling moment. The single rotor cancels the rolling moment by the half-wing, resulting in a lift-offset state. The results showed that the lift-offset due to the half-wing remarkably increased the effective lift-to-drag ratio of the rotor and the wing. The present authors suggested a differential flap system to control the lift-offset of the single rotor and showed to improve the effective lift-to-drag ratio through the numerical simulation [18]. The winged compound helicopters require the download reduction by a large flap system during hovering flight, and the differential flap system utilizes these flaps in forward flight.

This paper describes an experimental investigation of the effect of differential flaps on the overall aerodynamic performance of the winged compound helicopter. The wind tunnel test was conducted in 2m x 2m low-speed wind tunnel (LWT2) at Japan Aerospace Exploration Agency (JAXA) in November 2021. The experimental setup and experimental results to evaluate the single-rotor lift-offset with the differential flap system are described in this paper.

2. EXPERIMENTAL SETUP

2.1. Test Facility and Load Measurement

The wind tunnel test was performed at JAXA 2m x 2m closed circuit type low-speed wind tunnel (LWT2). The test section is 2m x 2m square cross section and 4m long. Wind speed can be set from 3 to 60 m/s continuously. The maximum wind speed is 67 m/s.

Figure 1 shows the experimental setup for the rotor/wing-body configuration. A closed cart is used, and the model is supported from downstream by a robot support system. The total forces and moments of the rotor and wing-body are measured using a sting type six-component balance (LMC 6522 38/Z200, NISSHO-ELECTRIC-WORKS CO,. LTD), as shown in Fig. 1. Time averaged forces and moments are measured. The sampling rate is 1 kHz, and the measurement time is 5 seconds (58 rotor revolutions at 700 RPM during the test).

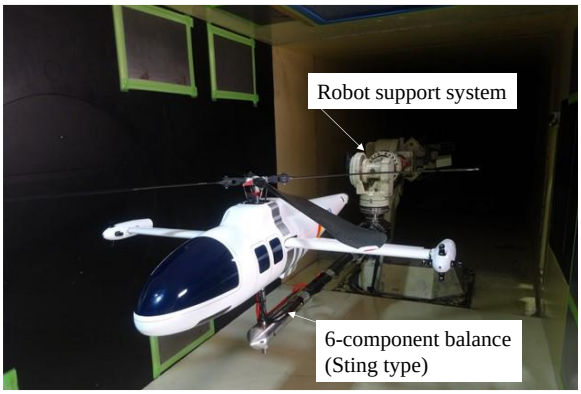

Figure 1. Experimental setup in test section at LWT2.

2.2. Test Model

The test model is based on a distinctive concept of a compound helicopter and a flyable radio-controlled rotorcraft is used [19]. This rotorcraft is a 1/7 scaled-down model and consists of a single main rotor, a wing-body including tail stabilizers, a pair of side propellers mainly for yaw control, and a tail propeller to achieve high-speed flight. The side/tail propellers and the tail stabilizers are removed in this test to focus on the aerodynamic performance of the rotor and the wing-body. The model has been modified to mount on the robot support system.

The main rotor is driven by a brushless motor and can rotate up to 2000 RPM. The rotor radius is 0.765 m, and the rotational direction is clockwise looking from above. The number of blades is four, and two types of rotor blades are tested to compare the

overall aerodynamic performance and the effect of lift-offset. UH-60A rotor blade [20-22] is used as the reference blade because of plenty of available published resources. Note that the UH-60A blade model is built to match the test model. Hence, the structural model is not scaled and only 3D geometry such as the airfoil and planform are reproduced. Another blade is the optimized blade, called high-μ rotor, designed for a high advance ratio at JAXA [23]. The high- μ rotor was designed based on the specifications of UH-60A, such as the maximum take-off weight, tip Mach number, and solidity (equivalent chord) using an efficient global optimization method. The objective functions for the optimization were the aerodynamic performance maximizations under hover and high advance ratio conditions. Three different blade tip shapes have been proposed. The baseline blade, high-μ BLN, is used in this study. The blades were constructed using CFRP composite materials. The blades used in the wind tunnel test are shown in Fig. 2, and the specifications of the blades are summarized in Table 1.

Figure 2. Blade model used in the wind tunnel test.
(Upper: UH-60A blade, Lower: high-μ BLN)

Table 1 Blade specifications.

Rotor radius	0.7665 m
Solidity	0.082
Root cutout	0.156 [/R]
Twist	UH-60A: nonlinear (-16° equivalent linear twist) high-μ BLN: nonlinear (within $\pm 2°$)
Airfoil	UH-60A: SC1095/SC1094R8 high-μ BLN: Ellipse/SC1095
Rotational direction	Clockwise

Streamlined shape of the fuselage is adopted to provide lower drag at high speeds than that of conventional helicopters. The wing planform is trapezoidal with a taper ratio of 0.8. There is no twist angle, the airfoil is NACA0015, and the incidence angle is $5°$. The wing has large flaps to reduce the download caused by the rotor downwash during hover. The flap type is the plain flap, the chord length of the flap is 40% of the wing chord length. The flap operating range is $-10°$ to $90°$ and the downward deflection of the flap trailing edge is defined positive. The wing-body specifications are summarized in Table 2.

Table 2 Wing-body specifications.

Longitudinal length of fuselage	1.380 m
Maximum diameter of fuselage	0.210 m
Span length of wing	0.994 m
Wing area	0.107 m^2
Wing chord (root, tip)	0.120, 0.096 m
Wing airfoil	NACA0015
Wing incidence	$5°$
Flap type	Plain flap
Chord length of flap	40% wing chord length
Flap operating rage	$-10°$ to $90°$

Differential flaps are pre-set before the test using a specific angle gauge, as shown in Fig. 3. The rolling moment on the wing-body is controlled by the difference in lift between the left and right wings. Since the lift-offset state generates more lift on the advancing side of the rotor, the flaps should be operated upward under the advancing side and downward under the retreating side. In this model, the rotor rotates in clockwise direction, so the left-side wing is under the advancing side, and the right-side wing is under the retreating side of the rotor, respectively.

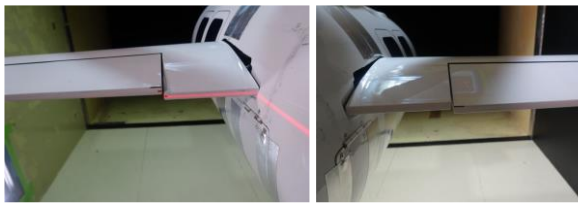

(a) flap up (left-side) (b) flap down (right-side)

Figure 3. Example of differential flap setting. ($\delta_f = \pm 2°$).

2.3. Test Conditions

Experiments were conducted to evaluate the aerodynamic performance of the isolated wing-body and the rotor/wing-body configurations. The test

conditions are shown in Tables 3 and 4. Test of the isolated wing-body configuration was performed to investigate the aerodynamic characteristics and the effect of the differential flaps. The wind speed is 50 m/s, and the Reynolds number based on the mean aerodynamic chord (MAC=0.108 m) is 3.7×10^5. The differential flap angles are determined from a previous study [18]. Test of the rotor/wing-body configuration was carried out to investigate the effect of the single-rotor lift-offset. The collective pitch angle was changed, and three advance ratios were investigated for two rotor blade types. The rotational speed of the main rotor was 700 RPM to simulate the high advance ratio up to 0.7. The advance ratios were set to 0.3, 0.5, and 0.7.

Table 3 Test condition for the isolated wing-body.

Wind speed	50 m/s
Angle of attack	-10°~15°
Flap angle	$0°, \pm1°, \pm2°, \pm3°, \pm4°, \pm5°$

Table 4 Test condition for the rotor/wing-body.

Rotor speed	700 RPM ($V_{tip} = 56.1$ m/s)
Advance ratio	0.3, 0.5, 0.7
Attitude angle	0°
	θ_0-sweep (0°~10°)
Rotor control	Tip-path plane parallel to the wind axis
Flap angle	$0°, \pm1°, \pm2°, \pm3°, \pm4°, \pm5°$

The rotor was controlled by referring to the total rolling moment at the six-component balance position during the test of the rotor/wing-body configuration. Also, the tip-path plane of the rotor was adjusted to be parallel to the wind axis. The six-component balance was located below the wing-body. The rolling moment measured at the balance includes the contributions by the side forces of the rotor and wing-body, which was about 1% to 5% of the total lift of the rotor and wing-body. The rotor cannot be controlled by the actual rolling moment at the rotor center during the test. This problem will be improved in future modifications of the test instruments.

Idealistically, the overall performance of the rotor and wing-body should be evaluated under nominal constant design lift condition at each flight condition. However, the wind speed determines the wing lift and the rotor advance ratio. As a result, it is difficult to match the target lift with both above parameters in present slowed-rotor test, especially under high-speed conditions. Therefore, the test conditions were set based on the lift-share ratios between the rotor and the fixed-wing. The lift-share ratio of the rotor significantly affects the aerodynamic interference between the rotor and the fixed-wing [9]. The target overall lift is estimated for each advance ratio of the rotor.

Flight conditions were determined based on the full-scale rotorcraft. Considering the drag divergence Mach number on the blade, the rotor rotational speed is slowed when the flight speed increases. The assumed RPM schedule of the main rotor is shown in Fig. 4. The rotor rotational speed is reduced from hover RPM (100% RPM) to 75% RPM finally. The Mach Number on the blade at the advancing side, called an advancing Mach number, is limited to less than 0.8 while reducing the rotational speed. Above the flight speed of Mach number of 0.15, rotor speed decreases linearly with flight speed toward 75% RPM so that the advancing Mach number does not exceed 0.8. In actual flight, the rotation speed reduction should consider the vibration of the rotor, avoiding the resonance frequencies. However, in this study, it is assumed that the rotor speed is linearly reduced for simplicity.

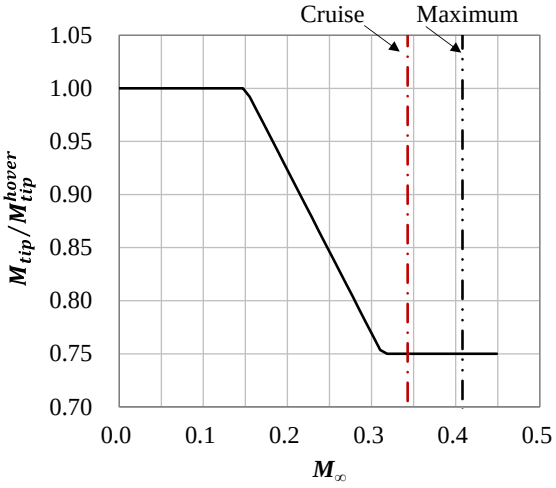

Figure 4. RPM schedule of the main rotor.

Figure 5 shows the assumed lift-share ratio between the rotor and wing-body for the advance ratio. The lift coefficient of the wing-body is obtained from the wind tunnel test, and the value is 0.346. The advance ratio in cruising flight is 0.7, and the lift-share ratio of the rotor is about 0.3 during cruising flight.

The target overall lift coefficient, C_L/σ, for the wind tunnel test obtained from the lift-share ratio of the rotor and the lift of the wing-body is calculated as

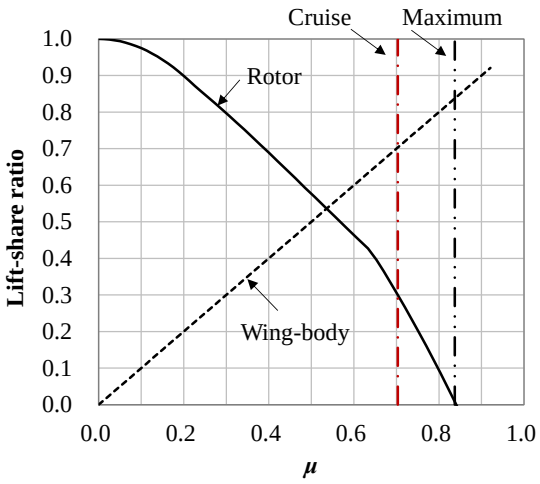

Figure 5. Lift-share ratio between the rotor and wing-body.

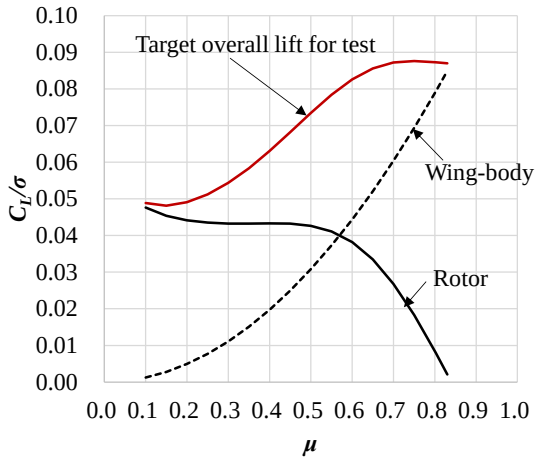

Figure 6. Target overall lift coefficient based on the designed lift-share ratio between the rotor and the wing-body.

shown in Fig. 6. The overall lift coefficient is described as follows.

$$C_L = \frac{L^{MR} + L^{WB}}{\rho\pi R^2(\Omega R)^2} \quad (1)$$

Where ρ is the air density, rotor disk area, πR^2, rotor radius, R, blade tip speed, ΩR. The superscripts of MR and WB indicate the main rotor and the wing-body, respectively.

Wind tunnel test were conducted by changing the collective pitch angle of the blade including the target overall lift coefficient as shown in Fig. 7. The target conditions at the advance ratio of 0.3, 0.5, and 0.7 are summarized in Table 5.

3. RESULTS

3.1. Data Processing

The total aerodynamic forces of the rotor and wing-body were measured using an internal sting six-component, as shown in Fig. 1. In this study, the moment center was converted to the rotor center from the balance and defined in the right-hand system, as shown in Fig. 8.

The measured data include the aerodynamic forces of the sting and hub. The tares of the sting and hub were removed from the measured data to evaluate the total aerodynamic performance of the rotor and wing-body. The tare data were measured in their individual configurations. Separate measurement of rotor and wing-body forces is future work. This paper evaluates the effect of differential flaps on the aerodynamic performance of the rotorcraft due to the

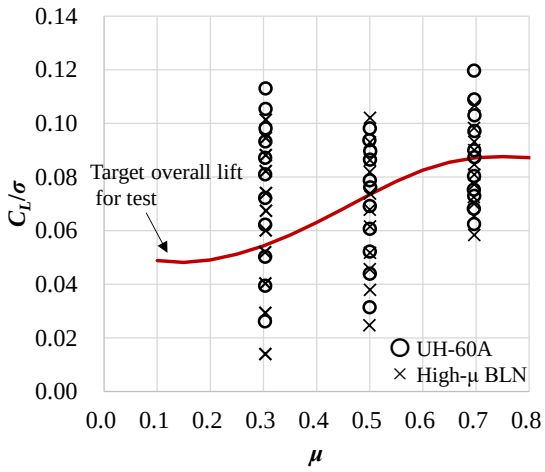

Fig. 7 Test envelope of the zero flap deflections. Symbols show the test conditions for both rotors. Red line indicates the target overall lift conditions.

Table 5 Target conditions.

Advance ratio	0.3, 0.5, 0.7
Lift-share ratio of the rotor	0.80, 0.58, 0.31
Target overall lift coefficient, C_L/σ	0.054, 0.073, 0.087

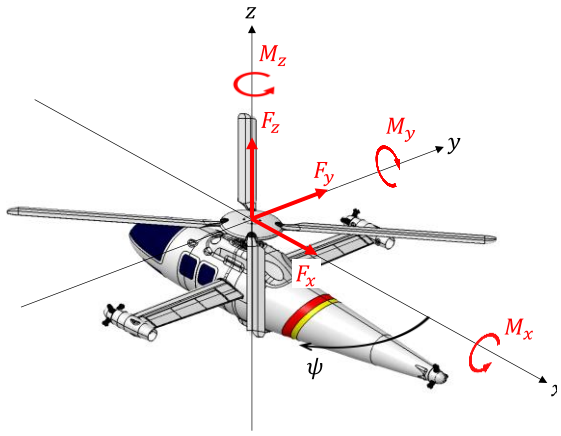

Figure 8. Definition of forces and moments.

differential flaps using the total rotor and wing-body forces.

The measured forces and moments are nondimensionalized based on the definition of Fig. 8 as follows.

$$C_D = \frac{F_x}{\rho\pi R^2(\Omega R)^2} \quad (2)$$

$$C_Y = \frac{F_y}{\rho\pi R^2(\Omega R)^2} \quad (3)$$

$$C_L = \frac{F_z}{\rho\pi R^2(\Omega R)^2} \quad (4)$$

$$C_{Mx} = \frac{M_x}{\rho\pi R^2(\Omega R)^2 R} \quad (5)$$

$$C_{My} = \frac{M_y}{\rho\pi R^2(\Omega R)^2 R} \quad (6)$$

$$C_{Mz} = \frac{M_z}{\rho\pi R^2(\Omega R)^2 R} \quad (7)$$

The lift coefficient includes the lift of the rotor and wing-body. In this test, the rotor thrust corresponds to the rotor lift because the rotorcraft attitude is zero during the test.

The overall aerodynamic performance is investigated using the effective lift-to-drag ratio, C_L/C_{DE}. The effective drag coefficient, C_{DE}, is utilized to evaluate the effective drag of the rotor and consists of the rotor drag and power. Since the measured data is the total force of the rotor and the wing-body, the overall effective drag is evaluated using the overall drag and yawing moment of the rotor and wing-body. The overall yawing moment includes the rotor torque and the yawing moment of the wing-body. The effective drag coefficient is computed as follows.

$$C_{DE} = \frac{C_P}{\mu} + C_D \quad (8)$$

$$C_P = \frac{(M_z^{MR} + M_z^{WB})\Omega}{\rho\pi R^2(\Omega R)^3} \quad (9)$$

$$C_D = \frac{F_x^{MR} + F_x^{WB}}{\rho\pi R^2(\Omega R)^2} \quad (10)$$

μ is the advance ratio of the rotor, $\mu = V\cos i/(\Omega R)$, where i is the incidence shaft angle of the rotor, which is zero here. The rotor torque in this test occurs as a positive yawing moment, which is very large relative to the yawing moment produced by the wing, as indicated by a previous study [7].

3.2. Effect of Differential Flap Deflections on the Aerodynamic Performances

The aerodynamic forces and moments versus the angle of attack of the isolated wing-body were measured. This section shows the effect of the differential flaps on the aerodynamic performance of the isolated wing-body at an attitude angle of zero degrees. The aerodynamic coefficients shown here utilize a nondimensionalization of a typical fixed-wing aircraft as shown below.

$$C_{L\infty} = \frac{F_z}{\frac{1}{2}\rho U^2 S} \quad (11)$$

$$C_{D\infty} = \frac{F_x}{\frac{1}{2}\rho U^2 S} \quad (12)$$

$$C_{Mx\infty} = \frac{M_x}{\frac{1}{2}\rho U^2 Sb} \quad (13)$$

$$C_{Mz\infty} = \frac{F_z}{\frac{1}{2}\rho U^2 S} \quad (14)$$

Where U is the wind speed, b is the span length of the wing, and S is the wing area. The moment center is also defined at the rotor center to investigate the effect of differential flaps on aerodynamics.

Figure 9 shows the lift coefficients of the wing-body for the differential flap angles. The lift coefficient increases up to the differential flap angle of 3 deg, with a maximum increase of about 2%. The lift coefficient decreases at the differential flap angles after 4 deg, which seems to be due to the separation on the flap. In a more detailed design, the stall characteristics on the flap should also be considered. The change of lift coefficient of the wing-body due to the differential flaps is relatively small, and this system has a small effect on the lift share ratio between the rotor and wing-body.

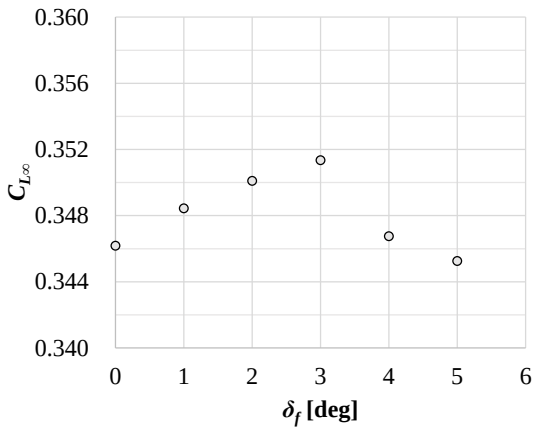

Figure 9. Lift coefficients of the wing-body for the differential flap angles.

Figure 10 shows the drag coefficients of the wing-body for the differential flap angles. It can be seen that the drag coefficient increases as the differential flap angle increases. Since flap actuation increases the profile and induced drags of the wing, the effect on overall performance should be considered when applying the differential flap system. In order to improve the overall rotorcraft performance by increasing rotor performance due to lift-offset, the performance degradation of the wing-body due to the

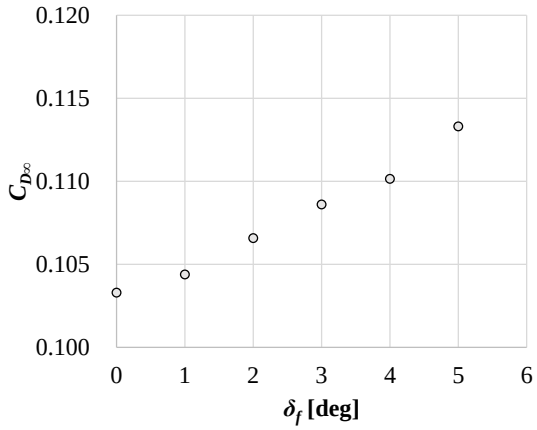

Figure 10. Drag coefficients of the wing-body for the differential flap angles.

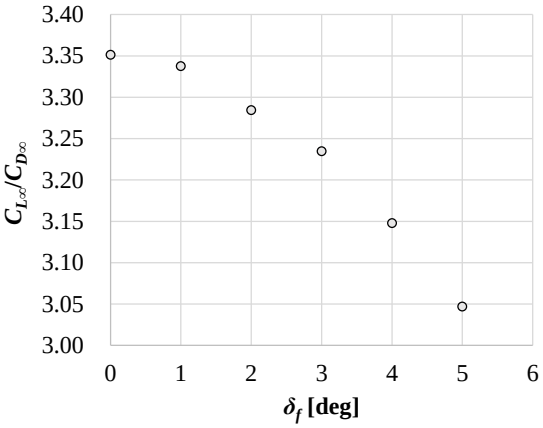

Figure 11. Lift-to-drag ratio of the wing-body for the differential flaps.

differential flap should be minimized.

Figure 11 shows the lift-to-drag ratios of the wing-body for differential flap angles. The lift-to-drag ratio at the differential flap angle of 3 deg is reduced about 3% relative to the zero flap angles, and at the differential flap of 5deg, 9% reduction relative to the zero flap angle. The lift-to-drag ratio of the rotor due to the lift-offset is expected to enhance by more than 20% [18]. Therefore, the rotor performance improves significantly than the decrease in wing-body performance due to the differential flaps. The overall performance is expected to improve due to the lift-offset.

Figure 12 shows the rolling moment coefficients of the wing-body for the differential flaps. The rolling moments are defined at the rotor center. The differential flaps contribute linearly to the increase in the rolling moment.

Figure 13 shows the estimated lift-offset, *LO*, for the differential flap angle at each advance ratio. The single-rotor lift-offset is defined as follows.

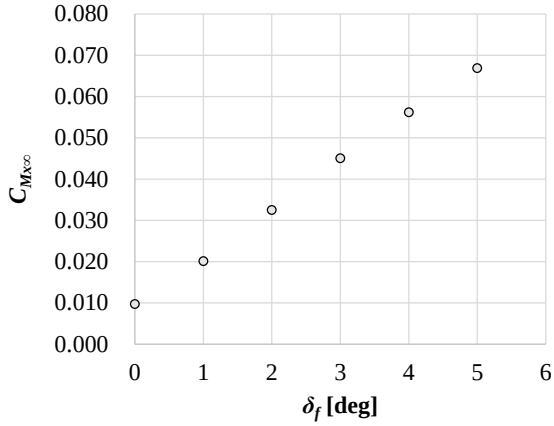

Figure 12. Rolling moment coefficients of the wing-body at the rotor center for the differential flaps.

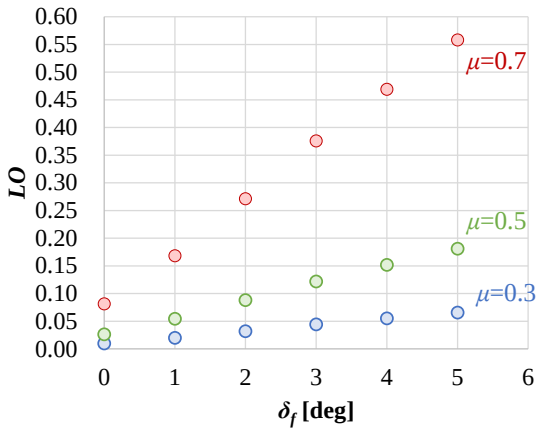

Figure 13. Estimated lift-offset, *LO*, for the differential flaps at each advance ratio.

$$LO = \frac{M_x^{MR}}{L^{MR}R} = \frac{C_{Mx}^{MR}}{C_L^{MR}} \quad (15)$$

The lift-offset values at each advance ratio are calculated based on the target design conditions. The rolling moment of the rotor, M_x^{MR}, is assumed to correspond to that of the wing-body. The estimated maximum lift-offset is 0.56 at the differential flap angle of 5 deg and the advance ratio of 0.7. However, this value is relatively larger than that of a coaxial rotor system. The lift-share ratio of the coaxial rotor is almost half between the upper and lower rotors, and the maximum lift-offset resulting from structural limitations have been reported to be 0.3 [10, 12]. Based on previous studies, the maximum rolling moment coefficient of the rotor can be estimated to be $0.15C_L^{MR}$ from Eq. (15). For the lift-share ratio of 0.3, the assumed maximum lift-offset is 0.5. Therefore, the test was conducted with caution at the differential flap angle of 5 deg, but the test could be conducted because the rotor thrust was smaller than the nominal design. However, the bending moment

generated around the hub should be paid attention when using the lift-offset technology.

Figure 14 shows the yawing moment coefficients of the wing-body due to the differential flaps. The actuation of the differential flaps between the right and left side wings creates a difference in the aerodynamic drag of the fixed-wings. The yawing moment is generated in the negative direction by the differential flap. This direction is opposite to the rotor torque; thus, the differential flap provides an adverse yaw effect. Therefore, the differential flap system reduces the required power for antitorque devices, such as side propellers.

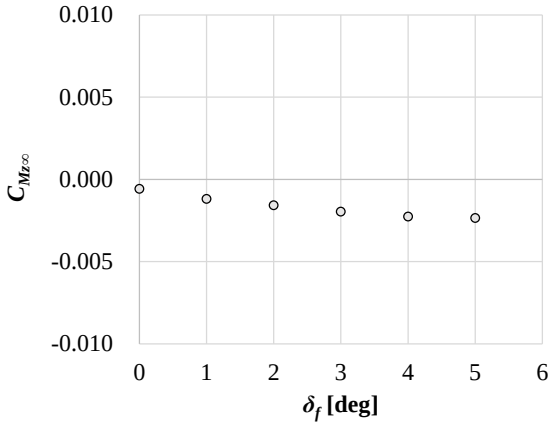

Figure 14. Yawing moment coefficients of the wing-body for the differential flaps.

3.3. Effect of Single-rotor Lift-offset

This section describes the effect of differential flaps on the total aerodynamic characteristics of the rotor and wing-body. The overall aerodynamic performance in three advance ratios was compared between two different blades, which are the UH-60A blade and High-μ BLN blade. The comparisons of aerodynamic characteristics at zero flap deflections are presented, and then the effect of the differential flaps on the overall performances is discussed.

3.3.1. Overall Performance with Zero Flap Deflections

Figure 15 shows the overall lift coefficients of the rotor and wing-body for the collective pitch angle in the advance ratios of 0.3, 0.5, and 0.7. The results for each blade of UH-60A and High-μ BLN are indicated by the difference in symbols, a circle symbol shows the UH-60A, and a cross symbol shows the High-μ BLN. The different colors indicate the results of each advance ratio; the blue, green, and red colors show the advance ratio of 0.3, 0.5, and 0.7.

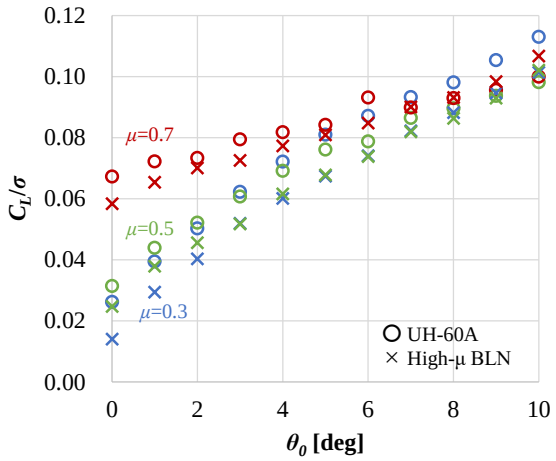

Figure 15. Overall lift coefficient for the collective pitch of the rotor with zero flap deflections at advance ratios of 0.3. 0.5, 0.7.

The overall lift coefficient at zero collective pitch angle increases with increasing rotor advance ratio, which is mainly due to the increase in the lift of wing-body. The sensitivity of the overall lift to the collective pitch angle of the rotor decreases in the high advance ratio condition. The sensitivity of rotor thrust to collective pitch angle is reduced, which has been shown experimentally in previous studies [24, 25]. The test results show similar trends to previous studies.

Figure 16 shows the overall lift-to-drag ratios against the overall lift coefficients with zero flap deflections at advance ratios of 0.3, 0.5, and 0.7. The maximum lift-to-drag ratio is obtained at an advance ratio of 0.3 and decreases with increasing advance ratio. High-μ BLN shows a higher overall lift-to-drag ratio than the UH-60A at each advance ratio, even though it was optimally designed at the advance ratio of 0.7.

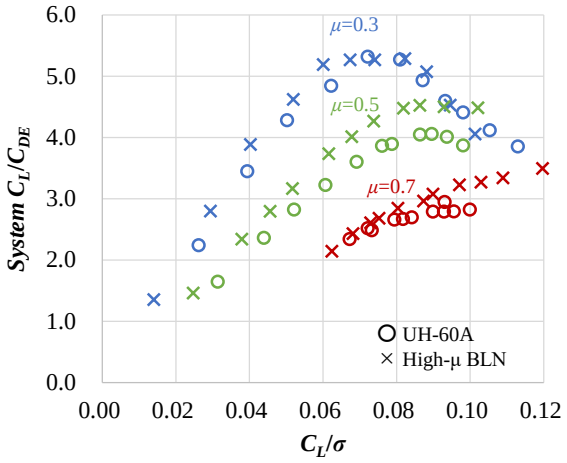

Figure 16. Overall lift-to-drag ratios against the overall lift coefficients with zero flap deflections at advance ratios of 0.3, 0.5, and 0.7.

Previous studies have shown that highly twisted blades, the UH-60A, have a significant aerodynamic interference effect on the fixed-wing in forward flight [18]. The rotor/wing aerodynamic interference causes a reduction of wing aerodynamic performance, which results in a decrease in overall performance [7, 9]. The High-μ BLN has less interference effect on the fixed-wing, and the performance is higher than UH-60A in high-speed conditions. Therefore, it is expected that the overall lift-to-drag ratios of High-μ BLN are higher than the UH-60A.

3.3.2. Effect on Differential Flaps on Overall Aerodynamic Characteristics at High Advance Ratio

The impact of lift-offset due to the differential flaps on aerodynamic characteristics is described using measured data with the advance ratio of 0.7. The test was conducted in the rotor and wing-body configuration, and the overall aerodynamic forces were measured while changing the collective pitch angle of the rotor.

Figure 17 shows the overall lift coefficients of the rotor and wing-body for the collective pitch angles with the differential flaps at the advance ratio of 0.7. The circle symbols using the rainbow color indicate the results of differential flaps. The blue color shows the result of differential flaps of ±1°, and the red color shows the result of differential flaps of ±5°. The black square symbols indicate the results of zero flap deflections.

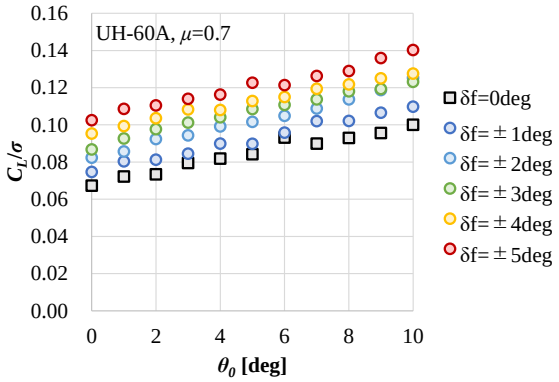

(a) UH-60A

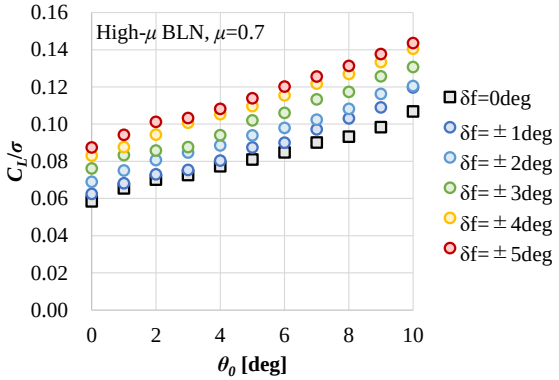

(b) High-μ BLN

Figure 17. Overall lift coefficients for the collective pitch angles due to the differential flaps at the advance ratio of 0.7.

The lift of the rotor is generated more on the advancing side with higher lift-offset ratios. The required collective pitch angle is reduced to obtain the same lift at the zero lift-offset condition. For both rotor blades, the overall lift coefficients at the same collective pitch angle increase with increasing differential flap angle, reflecting the effect of lift-offset. At all differential flap angles, the sensitivities of the overall lift coefficients to the collective pitch angles are nearly the same.

Figure 18 shows the overall drag coefficients for the overall lift coefficients due to the differential flaps at the advance ratio of 0.7. High-μ BLN has a relatively smaller overall drag coefficient than the UH-60A because of the small twist of the blade. At the same overall lift coefficient, the overall drag coefficient of the UH-60A blade is significantly reduced by the lift-offset, whereas it tends to increase for High-μ BLN. The drag of wing-body increases as the differential flap angle increases. The previous study has shown that the rotor drag decreases due to the lift-offset, but High-μ BLN has low drag, and it does not provide a significant drag reduction effect [18]. In High-μ BLN, the increase in the drag on the wing-body is considered to be more significant than the drag reduction effect of the lift-offset. Therefore, for the UH-60A, the reduction of rotor drag due to the lift-offset contributes significantly to the overall drag reduction. For High-μ BLN, the increase in wing-body drag due to the differential flaps contributes to the overall drag increase.

Figure 19 shows the overall power coefficients for the overall lift coefficients due to the differential flaps at the advance ratio of 0.7. The overall power coefficient is evaluated by the rotor torque and the yawing moment of the wing-body, as shown in Eq. (9). The overall power coefficients of both rotor blades decrease dramatically with increasing lift-offset due to the differential flaps, especially at the higher overall lift coefficients. The power coefficient of High-μ BLN is larger than that of the UH-60A. It is presumed that High-μ BLN has the lightly twist distribution and the induced drag at the blade tip is larger than the UH-60A.

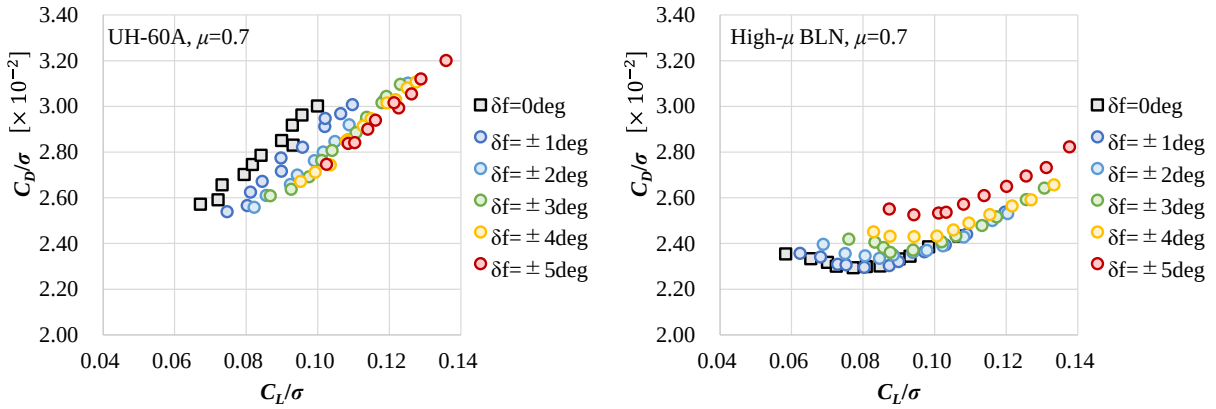

(a) UH-60A (b) High-μ BLN

Figure 18. Overall drag coefficients for the overall lift coefficients due to the differential flaps at the advance ratio of 0.7.

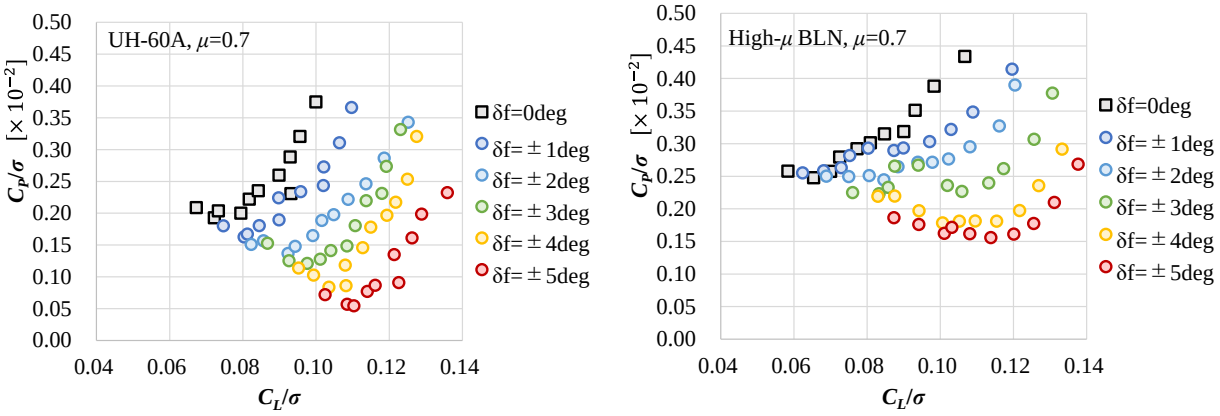

(a) UH-60A (b) High-μ BLN

Figure 19. Overall power coefficients for the overall lift coefficients due to the differential flaps at the advance ratio of 0.7.

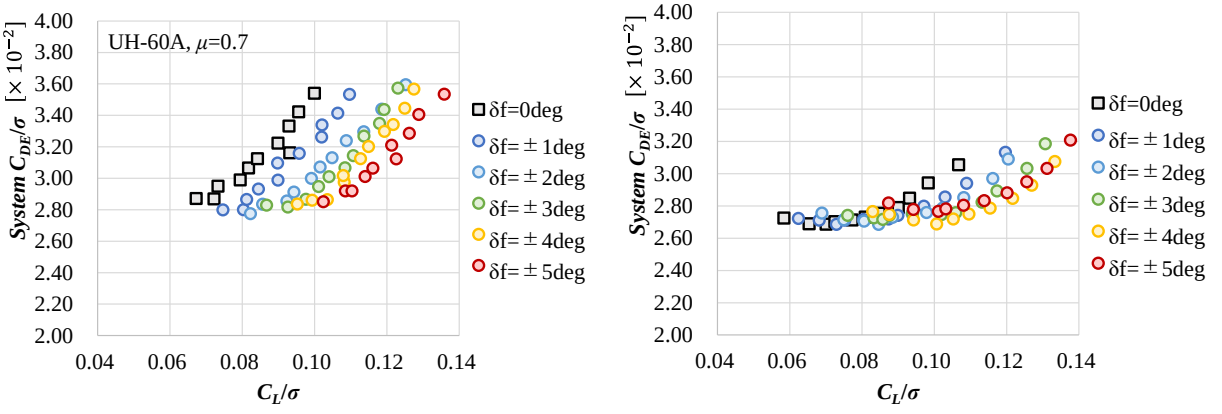

(a) UH-60A (b) High-μ BLN

Figure 20. Overall effective drag coefficients for the overall lift coefficients due to the differential flaps at the advance ratio of 0.7.

Figure 20 shows the overall effective drag coefficients for the overall lift coefficients due to the differential flaps at the advance ratio of 0.7. The overall effective drag coefficient of UH-60A is noticeably reduced where both the overall drag and power coefficients decrease. For High-μ BLN, the lift-offset with differential flaps has a certain reduction effect on the overall effective drag coefficient, and significant drag reduction is obtained at high overall lift coefficients.

The major difference between the UH-60A and High-μ BLN rotors, as mentioned above, is twist distribution in addition to the blade planform. From Fig. 18 to 20, the UH-60A rotor has the characteristics of the high sensitivity of effective drag coefficient to lift coefficient. On the other hand, High-μ BLN rotor has a relatively small sensitivity of the effective drag coefficient to the lift coefficient compared to UH-60A, which is a highly twisted blade. The high sensitivity of the effective drag coefficient to the lift coefficient is related to rapid performance changes. It is desirable to apply the lightly twisted blades to the high-speed rotorcrafts.

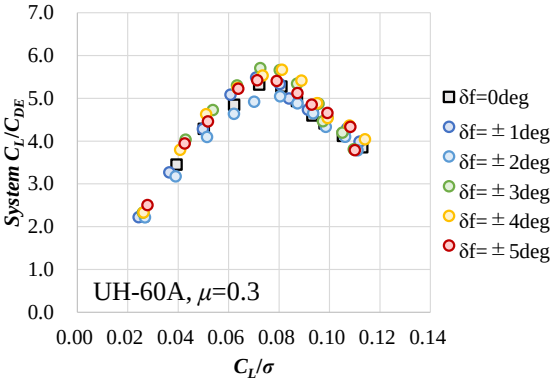

(a) $\mu = 0.3$

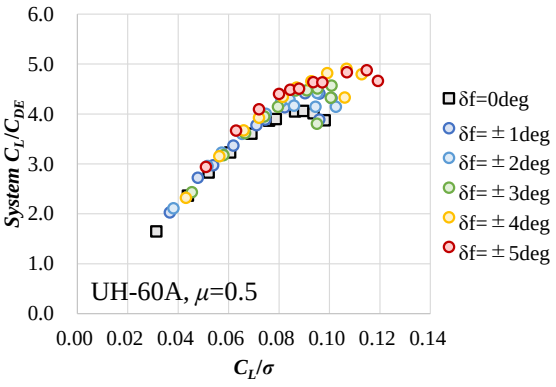

(b) $\mu = 0.5$

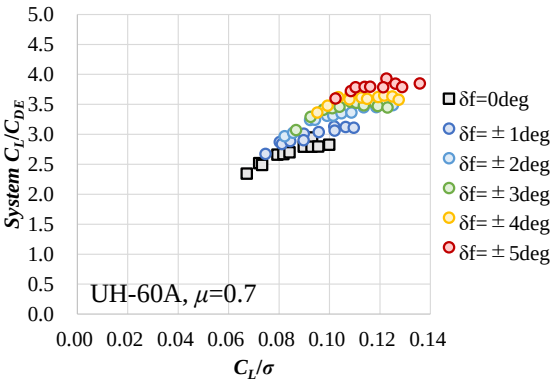

(c) $\mu = 0.7$

Figure 21. Overall effective lift-to-drag ratios due to the differential flaps against the overall lift coefficients for the UH-60A at the advance ratio of 0.3, 0.5, and 0.7.

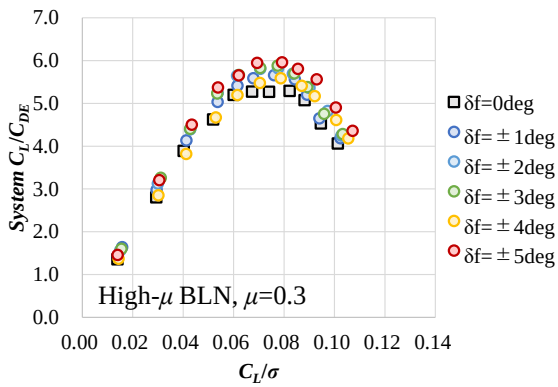

(a) $\mu = 0.3$

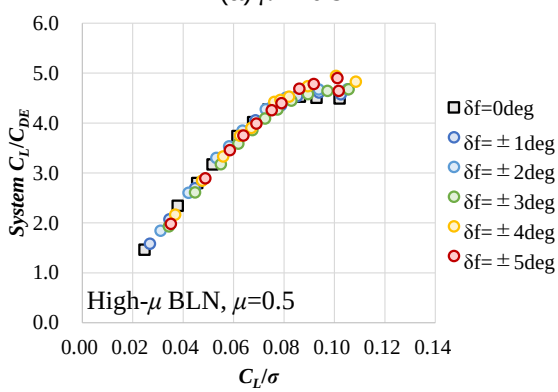

(b) $\mu = 0.5$

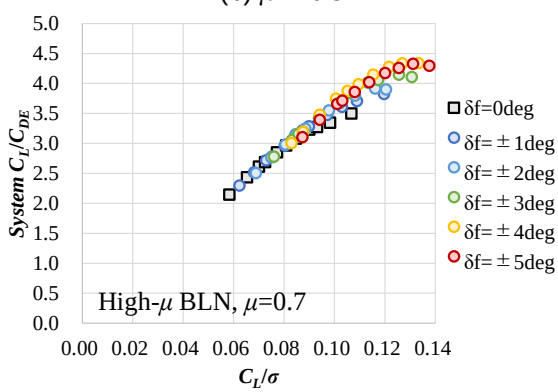

(c) $\mu = 0.7$

Figure 22. Overall effective lift-to-drag ratios due to the differential flaps against the overall lift coefficients for the High-μ BLN at the advance ratio of 0.3, 0.5, and 0.7.

3.3.3. Effect on Differential Flaps on Overall Effective Lift-to-Drag Ratio at Each Advance Ratio

The effect of lift-offset on the overall effective lift-to-drag ratio at the rotor advance ratio of 0.3, 0.5, and 0.7 is described. Figure 21 and 22 show the overall effective lift-to-drag ratios due to the differential flaps against the overall lift coefficients for the UH-60A and High-μ BLN rotors, respectively. The lift-offset due to the differential flaps is found to have a certain effect on performance improvement for the overall effective lift-to-drag ratio at each advance ratio. The impact on the performance improvement is particularly noticeable at the advance ratio of 0.7. At all advance ratios, the enhancement of the maximum lift-to-drag ratio at a higher overall lift coefficient is observed. Therefore, the lift-offset significantly increases the rotor performance under the higher thrust condition. Furthermore, the overall lift-to-drag ratios at the same lift coefficient improve due to the differential flaps.

Figure 23 shows the improvement of the effective lift-to-drag ratio at each differential flap from zero flap deflections for the target overall lift coefficients. Performance enhancement is obtained with lift-offset by the differential flaps on both blades. For the UH-60A, the overall effective lift-to-drag ratio at the advance ratio of 0.7 is improved by 10%. The performance reduction is observed at the advance ratio of 0.3. The amount of lift-offset is small under this condition, as shown in Fig. 13. The reason seems to be that the performance degradation of the wing-body is greater than the improvement of rotor performance due to the lift-offset. For High-μ BLN, the lift-offset due to the differential flaps contributes to the performance improvement. However, the overall effective lift-to-drag ratio slightly increases by about 2% at the advance ratio of 0.7 because the rotor thrust is only 30% of the target overall lift. Both blades are expected to achieve further performance improvements due to the lift-offset by the differential flaps with increased rotor thrust.

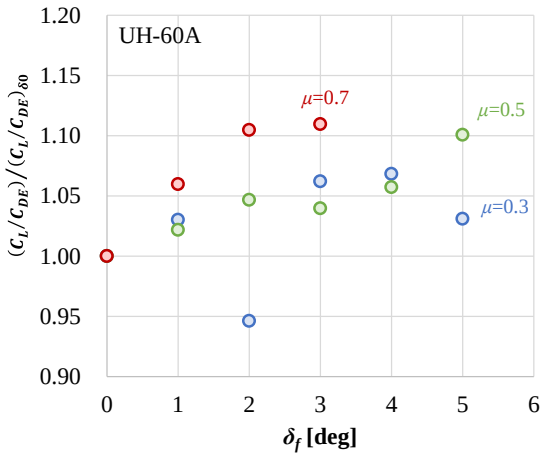

(a) UH-60A

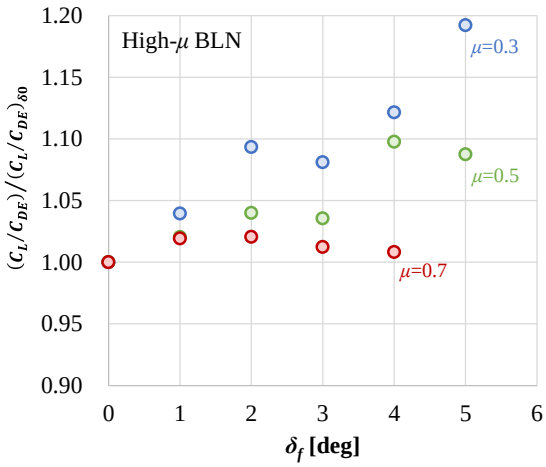

(b) High-μ BLN

Figure 23. Improvement of effective lift-to-drag ratio at each differential flap for the target overall lift coefficients.

4. CONCLUSION

Wind tunnel tests were conducted to investigate the single-rotor lift-offset system. The single-rotor lift-offset is achieved using flaps for download reduction on winged compound helicopters. The tests were conducted at JAXA 2m x 2m low-speed wind tunnel in the closed test section using a flyable radio-controlled model rotorcraft. The rotor rotational speed is set to 700 RPM to simulate high advance ratio conditions, and tests were performed at the advance ratio of 0.3, 0.5, and 0.7. Two types of rotor blades, which are the optimized rotor (High-μ BLN) designed at JAXA and the UH-60A rotor as the reference, are used to compare the effect of lift-offset on the overall aerodynamic performance. The following conclusions are obtained.

1. The single-rotor lift-offset due to the differential flaps enhances the effective lift-to-drag ratio. Although the performance improvement effects are different depending on the blade shape, the single-rotor lift-offset is experimentally demonstrated to have a certain impact on performance improvement.
2. The lift-offset due to the differential flaps reduces the required collective pitch angle to generate the same lift at the zero flap deflections. Therefore, it contributes to an increase in the maximum lift of rotorcrafts.
3. High-μ BLN, which was designed at advance ratio of 0.7, shows a higher overall lift-to-drag ratio than the UH-60A at each advance ratio.

Lightly twisted blades are effective as rotor blades for high advance ratio conditions because they provide low rotor drag.

4. The adverse yaw effect due to the differential flaps is observed from the results of isolated wing-body. This effect is expected to reduce the required power for the antitorque device, such as the side propeller on winged compound helicopters.

Acknowledgments

The authors gratefully acknowledge Ura Hiroki (JAXA) and the staff at JAXA 2m x 2m low-seed wind tunnel for the planning, preparation, and conducting of tests.

REFERENCES

[1] Tanabe, Y., Aoyama, T., Kobiki, N., Sugiura, M., Miyasita, R., Sunada, S., Kawachi, K., and Nagao, M., "A Conceptual Study of High Speed Rotorcraft," Proceedings of 40th European Rotorcraft Forum, Royal Aeronautical Soc. Paper 33-B, Southampton, UK, Sept. 2014.

[2] Blacha, M., Fink, A., Eglin, P., and Cabrit, P., "Clean Sky2: Exploring New Rotor craft High Speed Configurations," Proceedings of 43rd European Rotorcraft Forum, Associazione Italiana di Aeronautica e Astronautica Paper 593_ERF2017, Milan, Italy, Sept. 2017.

[3] Sheridan, P. F., and Smith, R. P., "Interactional Aerodynamics—A new Challenge to Helicopter Technology," Journal of the American Helicopter Society, Vol. 25, No. 1, Jan. 1980, pp. 3-21.

[4] Leishman, J. G., "The Helicopter, Thinking Forward, Looking Back," College Park Press, USA 2007.

[5] Brouwers, E., Fillmax, M., and Deresz, R., "Advanced AH-64 Compound Wind Tunnel Testing Overview," Proceedings of Vertical Flight Society 75th Annual Forum, Philadelphia, Pennsylvania, May 2019.

[6] Frey, F., Thiemeire, J., Öhrle, C., Keßler, M., and Krämer, E., "Aerodynamic Interactions on Airbus Helicopters' Compound Helicopter RACER in Cruise Flight," Proceedings of Vertical Flight Society 75th Annual Forum, Philadelphia, Pennsylvania, May 2019.

[7] Sugawara, H. and Tanabe, Y., "Numerical Investigation of Rotor/Wing Aerodynamic Interactions at High Advance Ratios," Journal of Aircraft, Vol. 56, No. 6, Nov.–Dec. 2019, pp. 2285-2298.

[8] Tanabe, Y., Sugawara, H., Kobiki, N., Kobayashi, W., Hayashi, H. and, Sato, R., "Experimental and Numerical Investigation of Interaction Between Rotor and Wing at High Advance Ratio," Proceedings of Vertical Flight Society 76th Annual Forum, Virtual, Oct. 5–8, 2020.

[9] Sugawara, H., Tanabe, Y., and Kameda, M., "Effect of Lift-Share Ratio on Aerodynamic Performance of Winged Compound Helicopter," Journal of Aircraft, Mar. 2021.

[10] Bagai, A., "Aerodynamic Design of the X2 Technology DemonstratorTM Main Rotor Blade," American Helicopter Society 64th Annual Forum, Montreal, Canada, April 29-May 2008.

[11] Walsh, D., Weiner, S., Arifian, K., Lawrence, T., Wilson, M., Millott, T., and Blackwell, R., "High Airspeed Testing of the Sikorsky X2 TechnologyTM Demonstrator," Proceedings of American Helicopter Society 67th Annual Forum, Virginia Beach, VA, May 2011.

[12] Johnson, W., "Influence of Lift Offset on Rotorcraft Performance," NASA/TP-2009-215404, Nov. 2009.

[13] Ho, J. C., and Yeo, H., "Analytical study of an isolated coaxial rotor system with lift offset," Aerospace Science and Technology, 100, 105818, 2020.

[14] Reddinger, J. and Gandhi, F., "Physics-Based Trim Optimization of an Articulated Slowed-Rotor Compound Helicoter in High-Speed Flight," Journal of Aircraft, Vol. 52, No. 6, Nov.–Dec. 2015, pp. 1756-1766.

[15] Wang, X., Maurya, S. and Chopra, I., "Slowed Hingeless Rotor Wind Tunnel Tests and Validation at High Advance Ratios," Journal of Aircraft, Vol. 58, No. 1, Jan.–Feb. 2021, pp. 153-166.

[16] Maurya, S., Wang, X., and, Chopra, I., "Wind Tunnel Test on a Slowed Mach-Scaled Hingeless Rotor with Lift Compounding," Proceedings of Vertical Flight Society 76th Annual Forum, Virtual, Oct. 5–8, 2020.

[17] Maurya, S., Chopra, I., and, Datta, A., "In Search of Extreme Limits if a Compound Helicopter in High Speed Flight," Proceedings of Vertical Flight Society 77th Annual Forum, Virtual, May 10–14, 2021.

[18] Sugawara, H. and Tanabe, Y., "Improvement of Aerodynamic Performance of a Winged Compound Helicopter due to Single-Rotor Lift-Offset," Proceedings of 47th European Rotorcraft Forum, Royal Aeronautical Society Paper #56, Conference Call, UK, Sept. 2021.

[19] Tanabe, Y., Sugiura, M., Kobiki, N. and Sugawara, H., "A New Concept of Compound Helicopter and Flight Tests," Proceedings of the 2018 Asia-Pacific International Symposium on Aerospace Technology (APISAT2018), Lecture Notes in Electrical Engineering, Vol. 459, Springer, Singapore, June 2019, pp. 1343-1352.

[20] Bousman, W. G., "Aerodynamic Characteristics of SC1095 and SC1094R8 Airfoils," NASA T2003-212265, AFDD/TR-04-003, Dec. 2003.

[21] Davis, S. J., “Predesign Study for a Modern 4-Blade Rotor for the RSRA,” NASA CR 166155, March 1981.
[22] Prouty, R.W., Helicopter Performance, Stability, and Control, Krieger, Malabar, FL, 2005, p. 698.
[23] Sugiura, M, Tanabe, Y., Sugawara, H., and Takekawa, K., “Optimal Design of Rotor Blade for a Winged Compound Helicopter at High Advance Ratio,” Proceedings of Vertical Flight Society 76th Annual Forum, Virtual, Oct. 5–8, 2020.
[24] Datta, A., Yeo, H., and Norman, T. R., “Experimental Investigation and Fundamental Understanding of a Slowed UH-60A Rotor at High Advance Ratio,” Proceedings of the American Helicopter Society 66th Annual Forum, Virginia Beach, VA, May 2011.
[25] Berry, B. and Chopra, I., “Slowed Rotor Wind Tunnel Testing of an Instrumented Rotor at High Advance Ratio,” Proceedings of 40th European Rotorcraft Forum, Southampton, UK, Sept. 2014.